HSRL Mixed Layer Heights README File
DISCOVER-AQ 2013
Houston, TX

Advisory

Given the variety of ways to define, retrieve, and use ML heights, as well as the difficulty in determining ML height in complex atmospheric conditions, the estimates of ML height and the height of the maximum aerosol gradient derived from the airborne HSRL measurements of aerosol backscatter may or may not be useful for a given application. **Therefore, we strongly recommend that users: 1) read the discussion below to learn about the methodology, and 2) examine the supplied imagery to gauge the suitability and uncertainty of these results.**

Directions

If you just want to know what is in the text files that provide the results, skip to Table 1 on page 6 at the end of this document. If you want to learn about the analysis that produced these results, read on. In the supplied images, the magenta lines represent one-minute running averages of the ML height. Site identification information for the DISCOVER-AQ campaigns are located in Table 2.

ML Heights Derived from the HSRL Data

Measurements acquired by the NASA Langley Research Center (LaRC) airborne High Spectral Resolution Lidar (HSRL) are used to examine the structure of the atmospheric boundary layer (BL). The term mixed layer (ML) height is appropriate for the measurement made by lidar (Hayden et al., 1997; Seibert et al., Stull, 1988; Tucker et al., 2009). Tucker et al. (2009), defines the ML height as the volume of atmosphere in which aerosol chemical species emitted within the BL are mixed and dispersed and since all measurements were collected during the daytime, this terminology is applicable to the airborne HSRL observations (Scarino et al., 2014).

ML heights from the daytime measurements were derived using an automated technique that uses a Haar wavelet covariance transform with multiple wavelet dilations (Brooks, 2003) to identify the sharp gradients in aerosol backscatter located at the top of the ML. Several studies have used techniques that employed such transforms to identify ML layer heights using lidar measurements (Davis et al., 2000; Cohn and Angevine, 2000). Although these techniques are effective where the vertical gradient is small within and above the ML and the inversion is sharp and well defined, these techniques can produce a bias in the ML height estimates when a gradient is present above or below the ML (Davis et al., 2000; Cohn and Angevine, 2000; Brooks 2003). Brooks (2003) attempted to eliminate this problem by developing an alternative technique that uses multiple wavelet dilations instead of a single dilation to identify the upper and lower limits of the backscatter transition zone and provide the altitude of the maximum in the covariance transform. This technique was found to be insensitive to mean vertical gradients in the background signal. Brooks (2003) demonstrated this technique using airborne backscatter lidar data acquired over relatively shallow marine boundary layers. We have used this technique and have found it works reasonably well under a variety of conditions.

We implemented this technique in the following manner. The algorithm used as input data the aerosol backscatter profiles (532 nm) derived from the HSRL measurements. These profiles are computed every 0.5 sec using a 10 second running average of the HSRL 532 nm backscatter data. Backscatter values are computed using 60 m vertical resolution, and are provided every 30 m. Clouds were screened from the analyses because they can produce signal gradients that can be misinterpreted by the wavelet algorithm as the ML top; furthermore because the cloud signal is typically very strong, any averaged profile that includes a cloud return will be dominated by the cloud return (Cohn and Angevine, 2000). When the laser pulse strikes a cloud, a large pulse is recorded at the

cloud top height. The laser pulse is attenuated by the cloud; the attenuation depends on the thickness and properties of the cloud. For typical BL cumulus clouds, little or no laser light penetrates below the cloud so that no useful laser return signals are measured in the atmosphere below the cloud. Therefore, in the images that follow, clouds are apparent as white objects with shadows below. Following Davis et al. (2000), we used the largest negative Haar wavelets to identify cloudy profiles.

The cloud-free backscatter profiles were then used in the wavelet covariance transform algorithm based on the method described by Brooks (2003). This algorithm computes a wavelet transform at multiple dilations (i.e. spatial distances) to compute the lower (H_1) and upper (H_2) limits of the transition zone as well as the altitude of the location of the maximum covariance (H_3). The relationship among the three altitudes and the lidar backscatter profile can be seen in more detail in Figure 1 which shows a single HSRL aerosol backscatter profile acquired at 19:40:13 UT on September 26, 2006 during the TexAQS/GoMACCS experiment. Davis et al. (1997) indicated that the depth (H_2-H_1) of this transition zone may be a better estimate of the entrainment zone depth than the area-averaged value usually defined. Note that Cohn and Angevine (2000) computed entrainment zone thickness as the distance between the 15th and 85th percentiles of the lidar-derived ML heights H_3. Therefore, in addition to providing H_1, H_2, and H_3, we have also provided heights corresponding to these percentiles computed over one-minute averages for each of H_1, H_2, and H_3. Brooks (2003) indicated that H_1, the lower limit of the transition zone, represents the top of the well-mixed layer. However, since Davis et al. (2000) and Cohn and Angevine (2000) used the altitude of the maximum covariance H_3 to identify the ML height, we will follow the same convention. We have computed and included all altitudes in the output file.

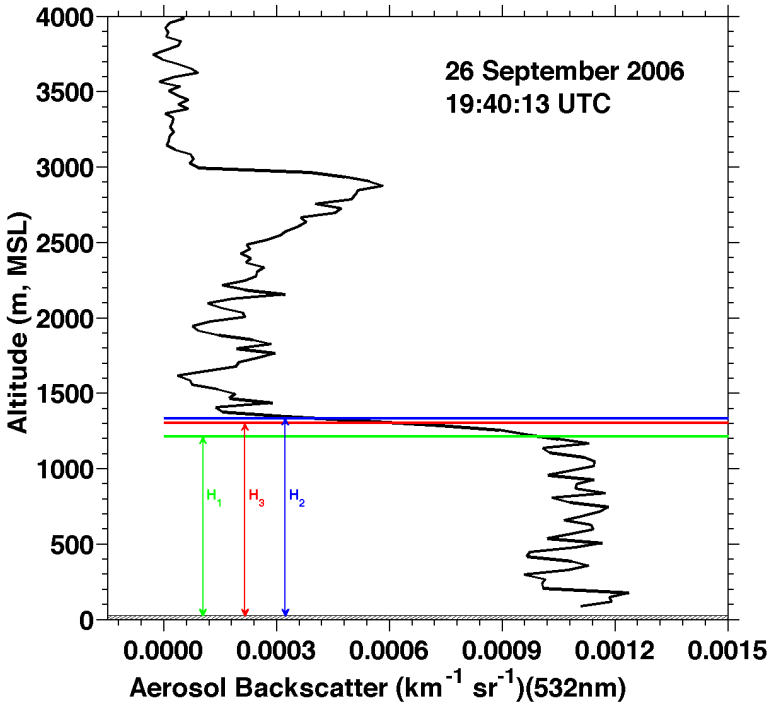

Figure 1. HSRL backscatter profile acquired at 19:40:13 UTC on 26 September 2006. The heights, H_1, H_2, and H_3, are derived from the modified Brooks algorithm.

Comparison of the initial algorithm results with the ML heights obtained from visual inspection revealed some limitations of the Brooks algorithm that we addressed by subsequent modifications. First, the algorithm would at times identify boundaries associated with elevated aerosol layers as the ML top. Consequently, the altitude region over which the algorithm searched for ML heights was limited to between H_1-500 m and H_2+500 m where H_1 and H_2 are the bottom and top heights of the transition zone computed using the previous minute of data. Because of the large changes of ML height between land and water, the results computed over water were not used as a basis for computing the results over land and vice versa. This restriction eliminated many of the false ML height detections.

Another modification was made to the algorithm to reduce the false detections due to elevated aerosol layers as well as noise in the lidar signal. We found that Brooks' algorithm, which is designed to choose the largest overall maximum value of the wavelet transform, would often erroneously pick an elevated aerosol layer above the apparent ML. Therefore, the algorithm was modified to look for local maxima greater than an empirically determined threshold value and choose the one at the lowest altitude. Examination of the heights from several flights shows that this modification produced results much closer to heights obtained by visual inspection.

An additional modification was made in the choice of dilation values used by the algorithm. The algorithm is designed to start with a small dilation that is on the order of the vertical data resolution (a_1~60 m) then increase the size of this dilation in an iterative manner to find the transition zone limits H_1 and H_2 as well as the altitude of maximum in the covariance transform H_3. Although this method provided good estimates of the transition zone limits, it often did not provide accurate estimates of H_3, when using the modification described above. The final "optimal" value of the dilation, a_2, which typically was about 200-300 meters, appeared to be too small to accurately capture the location of the maximum in the wavelet transform. Consequently, the algorithm was adjusted to use a third, larger dilation value, a_3, for determining H_3; a_3 was set to 900 m over land and 360 m over water. Thus, the optimal value of the dilation used to find H_3 appears to be a function of the ML height; the smaller values of the optimal dilation found by Brooks (2003) are likely due to the much shallower marine ML heights that were examined in this earlier study. In contrast, higher ML heights require larger values of this optimal dilation. Figure 2 shows an example of the aerosol backscatter profiles for the September 26, 2006 flight around the Houston area. The black lines represent one-minute running mean averages of H_1 and H_2 and the red line represents a one-minute running mean average of H_3. The ML top was easily identified by the algorithm as well as by visual inspection in this image.

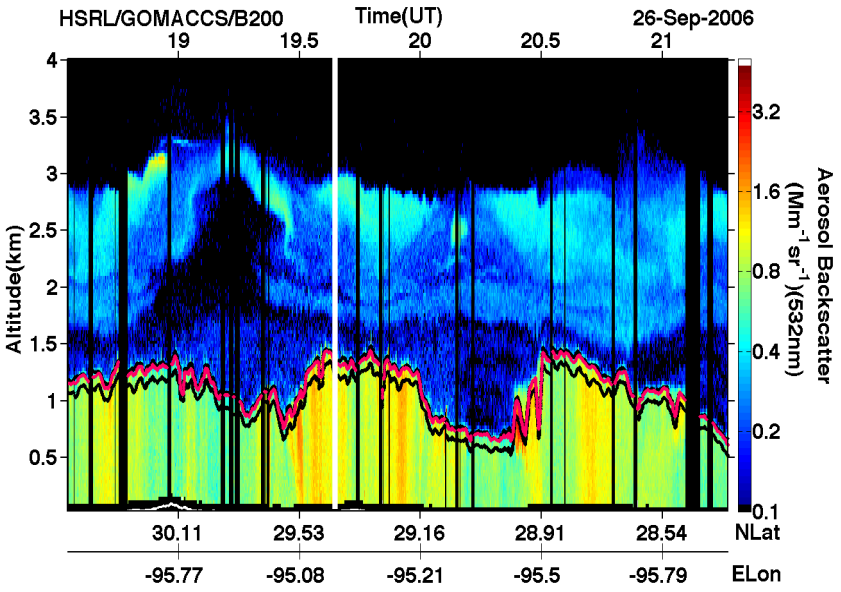

Figure 2. HSRL backscatter profile curtain on September 26, 2006. Black lines show one-minute running average bottom (H_1) and top (H_2) transition zone heights and the pink line shows the one-minute running average height of the maximum in the covariance transform of the Haar function. The vertical white line shows the location of the profile plotted in Figure 1.

Complicated aerosol structures within and/or above the ML or clouds at the top of the ML can prevent the algorithm from producing satisfactory results. As an example of such a case, Figure 3 shows the backscatter profiles for a portion of the flight near Washington D.C. on July 27, 2011. Note that the presence of aerosols above the ML complicates the determination of ML height and caused the algorithm to incorrectly identify the ML height during the first portion of this flight.

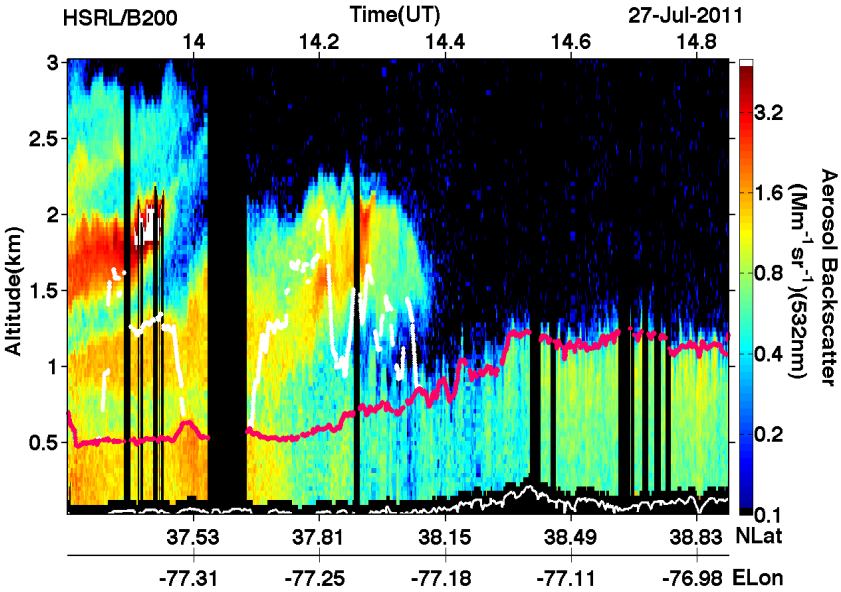

Figure 3. HSRL backscatter profile curtain on July 27, 2011. The white dots represent the ML height from the automated routine and the pink dots represent the "best estimate" ML height.

The magenta line in the image shows the location of the "best estimate" ML heights obtained by combining the algorithm results with the ML height obtained by visual inspection of the HSRL backscatter profiles.

Because the automated algorithm may not have produced satisfactory results for all times, each flight was manually examined and a second set of ML heights was produced by visually inspecting the backscatter image. The heights produced from the automated algorithm were also considered as part of this manual determination so this second set of "manual" heights is not entirely independent of the heights determined from the automated method. The H_3 altitudes determined from the automated algorithm and the ML heights determined from the manual inspection were combined to produce a set of "best estimate" ML heights. In those cases where the H_3 altitudes from the automated algorithm and manual altitudes were within 300 m, the H_3 altitudes from the automated algorithm were used as the best estimate; if the automated and manual altitudes differed by more than 300 m, the manual heights were used. Overall, during the TexAQS/GoMACCS experiment, the automated heights were chosen as the "best estimate" in about 85% of the cases examined during GoMACCS. (This success rate will vary depending on location, time of day, season, meteorology, etc.) Of these cases, the mean difference between the heights chosen by both methods differed by less than 10 m, so reducing the threshold used to decide which method to use would not have significantly changed the overall results. Further revisions of the algorithm did not appreciably increase the success rate of the automated algorithm results because of the complicated nature of aerosol and ML structures on several days. Indeed, in many of the cases where the automated algorithm failed to give satisfactory results, it was also difficult to accurately locate the ML height even by visual inspection.

Note that the ML derived in the manner discussed above may or may not correspond to the ML height derived from gradients in the potential temperature and/or trace gases such as water vapor. Figure 4 shows an example from a flight on July 2, 2011 during the DISCOVER-AQ mission. In this case, the ML height derived from the automated algorithm (shown by the pink line in the image on the left) matches the height corresponding to gradients in the profiles of potential temperature and water vapor as measured by coincident ozonesonde (shown by pink dotted line). However, the lidar aerosol backscatter imagery on this date shows that the height of the maximum aerosol gradient (shown in purple) sometimes occurred well above the ML height. Similarly, the radiosonde profiles show that the largest gradients in potential temperature and water vapor (shown by purple dashed line) occurred above the ML height. Since the height of the maximum aerosol gradient may provide a better indication of the depth of the aerosol layer (and perhaps also the relevant depth for trace gases), the altitude of the maximum aerosol gradient has also been computed and provided. **We emphasize that in some cases, the**

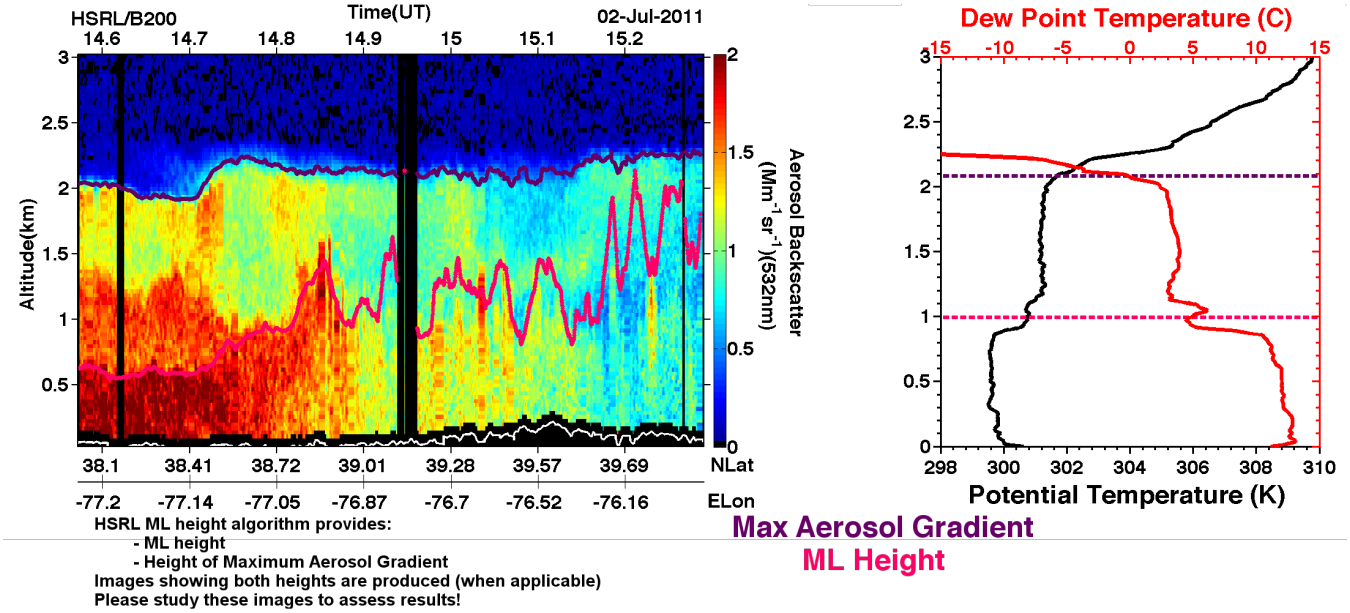

Figure 4. (left) HSRL backscatter profile curtain on July 2, 2011. (right) Ozonesonde profile of potential temperature and dew point from the Beltsville, MD site at about 15 UTC on this day (corresponding to oval on the lidar image).

lidar measurements of aerosol backscatter may not provide suitable estimates of the ML height and/or the height of the maximum aerosol gradient. Therefore, we strongly recommend that users study the supplied imagery to gauge the suitability and uncertainty of these results.

The results from both the manual and automated algorithm methods for all of the daytime flights are provided. Table 1 lists the parameters contained in this file. Note that there are several altitudes listed in the file to help provide more complete information regarding these results. All of the ML layer heights and transition zone heights are listed as altitude above ground level. Ground level elevation above sea level, which is also provided in the file, was determined from the Global Land One-km Base Elevation (GLOBE) Digital Elevation Map (DEM) database (http://www.ngdc.noaa.gov/mgg/topo/globe.html) based on the latitude and longitude recorded by the Global Positioning System (GPS) navigation system on the aircraft. GLOBE DEM ground elevation values were found to agree with the ground elevation determined from cloud-free HSRL profiles to within the 30 m spacing of the recorded HSRL signals. Values of H_1, H_2, and H_3 for each 0.5 sec, cloud-free profile are listed in the file. ML heights derived from manual inspection, interpolated to the 0.5 sec backscatter resolution, are also listed. The "optimal" dilation values (a_2) computed by the Brooks algorithm are listed. One-minute (~6 km at nominal aircraft speed) running mean averages of H_1, H_2, and H_3 are provided. We have also provided heights corresponding to the 15^{th} and 85^{th} percentiles computed over one-minute averages for each of H_1, H_2, and H_3. The "best estimate" ML heights are provided at 0.5 sec resolution as well as one-minute running mean averages. The altitudes of the maximum aerosol gradients are listed as well as one-minute running mean averages of these heights.

Contacts:

Richard Ferrare (Richard.A.Ferrare@nasa.gov)
Sharon Burton (Sharon.P.Burton@nasa.gov)
Amy Jo Scarino (Amy.Jo.Scarino@nasa.gov)

References

Brooks, I. M.: Finding boundary layer top: Application of wavelet covariance transform to Lidar backscatter profiles, J. Atmos. Ocean. Tech., 20, 1092–1105, 2003.

Cohn, S. and Angevine, W.: Boundary Layer Height and Entrainment Zone Thickness Measured by Lidars and Wind-Profiling Radars. J. Appl. Meteorol., 39, 1233-1247, 2000.

Davis, K. J., Lenschow, D. H., Oncley, S. P., Kiemle, C., Ehret, G. and Giez, A.: The role of entrainment in surface-atmosphere interactions over the boreal forest. J. Geophys. Res. – Atmos., 102, 29219-29230, 1997.

Davis, K. J., Gamage, N., Hagelberg, C. R., Kiemle, C., Lenschow, D. H., and Sullivan, P. P.: An Objective Method for Deriving Atmospheric Structure from Airborne Lidar Observation. J. Atmos. Ocean Tech., 17, 1455-1468, 2000.

Hayden, K. L., Anlauf, K. G., Hoff, R. M., Strapp, J. W., Bottenheim, J. W., Wiebe, H. A., Froude, F. A., Martin, J. B., Steyn, D. G., and McKendry, I. G.: The Vertical Chemical and Meteorological Structure of the Boundary Layer in the Lower Fraser Valley during PACIFIC '93. Atmos. Environ., 31, 2089-2105, 1997.

Seibert, P., Beyrich, F., Gryning, S. E., Joffre, S., Rasmussen, A., and Tercier, P.: Review and intercomparison of operational methods for the determination of the mixing height. Atmos. Environ., 34, 1001-1027, 2000.

Stull, R. B.: An Introduction to Boundary Layer Meteorology. Atmospheric Sciences Library, Kluwer Academic Publisher, Dordrecht-Boston-London, 666 pp., 1988.

Scarino, A.J., M. D. Obland, J. D. Fast, S. P. Burton, R. A. Ferrare, C. A. Hostetler, L. K. Berg, B. L. Lefer, C. L. Haman, R. R. Rogers, C. F. Butler, A. L. Cook, and D. B. Harper: Comparison of Mixed Layer Heights from Airborne High Spectral Resolution Lidar, Ground-based Measurements, and the WRF-Chem Model during CalNex and CARES, Atmos. Chem. Phys. Discuss., 14(11), 5547-5560, doi:10.5194/acpd-14-5547-2014, 2014.

Tucker, S. C., Brewer, W. A., Banta, R. M., Senff, C. J., Sandberg, S. P., Law, D. C., Weickmann, A. M., and Hardesty, R. M.: Doppler Lidar Estimation of Mixing Height Using Turbulence, Shear, and Aerosol Profiles. J. Atmos. Ocean Tech., 26, 673-688, 2009.

Those that have referenced our ML heights in their papers

Baker, K. R., Misenis, C., Obland, M. D., Ferrare, R. A., Scarino, A. J., and Kelly, J. T.: Evaluation of surface and upper air fine scale WRF meteorological modeling of the May and June 2010 CalNex period in California, Atmospheric Environment, doi:10.1016/j.atmosenv.2013.08.006, 2013.

Fast, J. D., Gustafson Jr., W. I., Berg, L. K., Shaw, W. J., Pekour, M., Shrivastava, M., Barnard, J. C., Ferrare, R. A., Hostetler, C. A., Hair, J. A., Erickson, M., Jobson, B. T., Flowers, B., Dubey, M. K., Springston, S., Pierce, R. B., Dolislager, L., Pederson, J., and Zaveri, R. A.: Transport and mixing patterns over Central California during the carbonaceous aerosol and radiative effects study (CARES), Atmos. Chem. Phys., 12, 1759-1783, doi:10.5194/acp-12-1759-2012, 2012.

Turner, D. D., Ferrare, R. A., Wulfmeyer, V., and **Scarino, A. J.**: Aircraft Evaluation of Ground-based Raman Lidar Water Vapor Turbulence Profiles in Convective Mixed Layers, *J. Atmos. Oceanic Technol.*, **31(5)**, 1078–1088, doi: 10.1175/JTECH-D-13-00075.1, 2014.

Table 1. Parameters listed in the HSRL ML height ascii files

Column	Colume Name	Units	Description
	Date		YYYYMMDD
1	Time	Decimal hours	UT time read from aircraft GPS for each record.
2	Latitude	Degrees (>0 north)	Latitude read from aircraft GPS for each record. (+North, -South)
3	Longitude	Degrees (<0 west)	Longitude read from aircraft GPS for each record. (+East, -West)
4	SiteID		Ground Sites (when HSRL was within 5 km of site) – see Table 2
5	Ground_Alt	m (MSL)	Ground altitude above mean sea level based on the one-km GLOBE Digital Elevation Map dataset based on the GPS latitude and longitude values. (0.5 sec resolution)
6	ML_height_AGL	m (AGL)	"H3" parameter from Brooks (2003). This is the altitude of the local maximum in the covariance transform of the Haar function (i.e. the maximum in the wavelet covariance) believed to be the mixed layer top. This height, and the remaining heights, are above ground level (AGL). (0.5 sec resolution)
7	H1_AGL	m (AGL)	"H1" parameter from Brooks (2003). Height of the base of the transition layer. (0.5 sec resolution)
8	H2_AGL	m (AGL)	"H2" parameter from Brooks (2003). Height of the top of the transition layer. (0.5 sec resolution)
9	Manual_ML_AGL	m (AGL)	Height of the mixed layer derived from manual inspection of the HSRL backscatter images.
10	AerThresh		Aerosol threshold used for most missions and is constant
11	AerActual		The value of the local maximum in the covariance transform corresponding to ML_height_AGL.
12	Minute_mean	m (AGL)	Running 1 minute average of ML_height_AGL
13	Minute_stddev	m	Standard deviation of the 1 minute average of ML_height_AGL
14	Minute_15pctl	m (AGL)	Height of the 15th percentile of the PBL_height_AGL parameter for each minute (i.e. 15% of the H3 heights are less than or equal to this height)
15	Minute_85pctl	m (AGL)	Height of the 85th percentile of the ML_height_AGL parameters for each minute (i.e. 85% of the H3 heights are less than or equal to this

			height)
16	Dilation	m	Optimal dilation (i.e. spatial extent) of the Haar function as determined by Brooks (2003) algorithm.
17	Minute_mean_h1	m (AGL)	Running 1 minute average of H1_AGL
18	Minute_15pctl_h1	m (AGL)	Height of the 15th percentile of the H1_AGL parameter for each minute (i.e. 15% of the H1 heights are less than or equal to this height)
19	Minute_85pctl_h1	m (AGL)	Height of the 85th percentile of the H1_AGL parameter for each minute (i.e. 85% of the H1 heights are less than or equal to this height)
20	Minute_mean_h2	m (AGL)	Running 1 minute average of H2_AGL
21	Minute_15pctl_h2	m (AGL)	Height of the 15th percentile of the H2_AGL parameter for each minute (i.e. 15% of the H2 heights are less than or equal to this height)
22	Minute_85pctl_h2	m (AGL)	Height of the 85th percentile of the H2_AGL parameter for each minute (i.e. 85% of the H2 heights are less than or equal to this height)
23	Best_ML_height	m (AGL)	"best estimate" of the ML height based on ML_height_AGL and Manual_ML_AGL. (0.5 sec resolution) (equal to ML_height_AGL when abs(ML_height_AGL-Manual_ML_height)<300 m; otherwise set to Manual_ML_height)
24	Best_Min_ML	m (AGL)	Running 1 minute average of Best_ML_height
25	Max_gradient	m (AGL)	Height of the global maximum of the wavelet transform AGL. May be above reported ML_height_AGL.
26	Minute_max	m (AGL)	Running 1 minute average of Max_gradient.

Table 2. Ground Sites in Houston, Texas Region

Site ID #	Site Name	Latitude	Longitude
101	Galveston	29.254474	-94.861289
102	Manvel Croix	29.520427	-95.392522
103	Smith Point	29.546244	-94.786969
104	Deer Park	29.670046	-95.128485
105	Univ. of Houston/Moody Tower	29.7177	-95.3416
106	Channel View	29.8025	-95.125556
107	West Houston	29.833056	-95.656944
108	Conroe	30.350278	-95.425